I&EC research
Industrial & Engineering Chemistry Research
pubs.acs.org/IECR
Article

Synergistic Catalysis of Brønsted Acid, Al-Lewis Acid, and Zn-Lewis Acid on Steam-Treated Zn/ZSM-5 for Highly Stable Conversion of Methanol to Aromatics

Tingjun Fu,* Chuntao Cao, Liangliang Zhang, Li Zhang,* Qian Ma, Zhenjun Xu, Ran Wang, Han Li, and Zhong Li*

Cite This: *Ind. Eng. Chem. Res.* 2023, 62, 1865−1876

Read Online

ACCESS | Metrics & More | Article Recommendations | Supporting Information

ABSTRACT: The development of stable and selective ZSM-5 catalysts for methanol aromatization remains an ongoing challenge. Here, we demonstrate highly stable aromatization on ZSM-5 by preliminary steam treatment before Zn introduction. Steam treatment destroyed part of frameworks, which decreased acid density from 0.5 to 0.25 mmol g^{-1} and increased Al-Lewis acid sites (Al-LAS) at the expense of Brønsted acid sites (BAS). However, aromatization activity was further increased and the lifetime was still kept at 100 h. A comparative experiment found that increasing the SiO_2/Al_2O_3 ratio from 60 to 240 also decreased acid density to 0.25 mmol g^{-1}, but BAS-based acid sites aggravated coke formation and reduced lifetime to 50 h. This reflected that Al-LAS and BAS on steam-treated ZSM-5 provided synergistic catalysis for stable aromatization. Introducing Zn into steam-treated ZSM-5 further transformed part of BAS to Zn-LAS but not changed acid density, which determined increased aromatics selectivity and a quite different well-maintained stability.

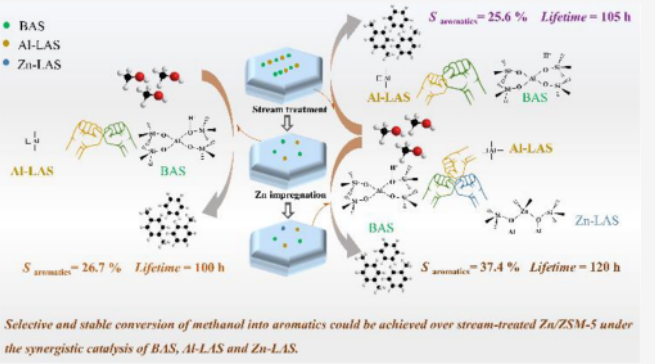

Selective and stable conversion of methanol into aromatics could be achieved over stream-treated Zn/ZSM-5 under the synergistic catalysis of BAS, Al-LAS and Zn-LAS.

INTRODUCTION

Light aromatics are widely used in dyes, perfumery, pharmaceuticals, and synthetic rubber, which are the most important basic raw materials for organic chemical industry.[1−3] It is anticipated that the aromatics market around the world is likely to reach a value of USD 29,012 billion by 2025.[4] Traditional aromatics production is mainly based on petroleum processing routes, such as naphtha reforming and thermal cracking of crude oil.[1,5−7] In view of the shortage and price volatility of petroleum resources, methanol conversion to aromatics (MTA) is now considered as a potential non-petroleum route to obtain aromatics, as methanol could be easily produced via syngas from a variety of carbon-containing sources, such as biomass, coal, natural gas, or even CO_2.[4,8]

The conversion of methanol to aromatics is catalyzed by an acidic catalyst and is a complicated reaction process including the dehydration of methanol, formation of hydrocarbon pool, and the production of aromatics via polymerization, hydrogen transfer, cyclization, and dehydrogenation.[9,10] During these reactions, some byproducts including light olefins and paraffins could also be formed, which influences the aromatics selectivity. Due to the advantages of large specific surface area, good hydrothermal stability, and adjustable acidity, ZSM-5 is considered as the preferred acidic catalyst for the selective conversion of methanol to aromatics.[11−14] Especially, because of the existence of special straight pores (0.53−0.56 nm) and zigzag pores (0.51−0.55 nm), high aromatics selectivity can be achieved because of this kind of shape-selective micropores for light aromatics[15−17] However, severe diffusion limitation in micropores could occur during reaction, which can slow down the diffusion of coke precursors and promote the coke formation via continuous polymerization of aromatic species[14,18−20] As the reaction proceeds, the formed coke could easily cover the acid sites and even block the micropores, which results in the quick deactivation of the catalyst.[21,22] Therefore, frequent regeneration is usually required to recover the activity of the catalyst in the process of industrial production, and a large amount of energy is consumed and the cost of aromatics synthesis is also accordingly increased. To promote the rapid removal of coke precursors and slow down the coke formation, many studies including alkali treatment, template induction, crystal size regulation, and morphology

Received: October 26, 2022
Revised: January 11, 2023
Accepted: January 11, 2023
Published: January 23, 2023

https://doi.org/10.1021/acs.iecr.2c03873
Ind. Eng. Chem. Res. 2023, 62, 1865−1876

control have been widely implemented for the optimization of molecule diffusion in micropores.[23−25]

Importantly, the acid properties of the ZSM-5 catalyst, such as acid types and acid densities, also strongly determine the product selectivity and catalytic stability. Bi et al.[9] had found that methanol could be first converted into low hydrocarbons over Brønsted acid sites (BAS) or Lewis acid sites (LAS). The formed light olefins could be converted into naphthenes over BAS-based cyclization. The further conversion of naphthenes to aromatics could be achieved by two routes.[9] One route is the hydrogen transfer process catalyzed by Brønsted acid sites. However, alkanes could also be formed during the formation of aromatics, which impedes the improvement of aromatics selectivity. Another route is the dehydrogenation process catalyzed by metal-Lewis acid sites, which only produces hydrogen as a byproduct and greatly improves the aromatics selectivity. Therefore, it is the synergy between Brønsted acid sites and metal dehydrogenation species that determines the total aromatic selectivity of the MTA reaction.

The acid types of ZSM-5 could be adjusted by introducing additives, such as Zn, Ca, Ni, Co, and Ag.[26−32] Among them, Zn species with good dehydrogenation performance and low price were widely used. Pinilla-Herrero et al.[33] found that the BAS density was decreased from 0.91 to 0.20 mmol g^{-1} by loading Zn on ZSM-5 with a SiO_2/Al_2O_3 ratio of 30, which was due to the fact that Zn^{2+} could balance the negative charge on part of the zeolite framework. The formed Zn-LAS increased the LAS density from 0.34 to 1.50 mmol g^{-1} and the aromatics selectivity increased from 11 to 31%. However, the introduction of Zn species not only enhanced the formation of aromatics but also increased the diffusion limitation of reactants and products, which was due to the occupation of Zn species in the micropores of ZSM-5, thereby reducing the catalytic life.[25] In addition, increasing acid density could promote aromatization processes such as hydrogen transfer and cyclization and improve aromatics selectivity, but the coke formation is also promoted at the same time, which could reduce catalytic stability.[34,35] Although many studies have been focused on the effect of acid properties on MTA performance, the development of stable and selective ZSM-5 catalysts remains a challenge.

Our previous study about the evolution of acid properties of ZSM-5 during reaction found that although the acid density was significantly reduced from 0.41 to 0.19 mmol g^{-1} after just 9 h, good stability with high aromatic selectivity was still presented in the next 50 h.[36] In view of the fact that the formed steam with high temperature during reaction could remove part of the aluminum structure, the acid density and acid types could be changed. Therefore, there is a strong possibility that the special acid density and type for steam-treated ZSM-5 determined stable methanol aromatization. Here, to confirm this positive effect of the steam treatment on acid modulation and the final structure−activity relationship, a nanosized ZSM-5 with a SiO_2/Al_2O_3 ratio of 60 was pretreated with hot steam and then used as the parent sample for Zn modification. In particular, ZSM-5 catalysts with the same acid density but different acid types were comparatively prepared by regulating the SiO_2/Al_2O_3 ratio and introducing Zn to study the synergistic catalysis of BAS, Al-LAS, and Zn-LAS. It was found that based on their synergistic catalysis of three types of acid sites, highly stable methanol aromatization was achieved on ZSM-5 prepared by preliminary steam treatment before Zn introduction. This study is expected to provide a theoretical guidance for understanding the key factors affecting the stable conversion of methanol to aromatics and for the directional preparation of catalysts from the point of view of acidic properties.

EXPERIMENTAL SECTION

Catalyst Synthesis. The parent nano-ZSM-5 zeolite with a SiO_2/Al_2O_3 ratio of 60 was synthesized following a reported method.[37] The synthesis materials were tetraethoxysilane (TEOS), tetrapropylammonium hydroxide (TPAOH, 25 wt %), sodium hydroxide, aluminum nitrate solution, and distilled water. The molar composition was 60 SiO_2:Al_2O_3:15TPAOH:15Na_2O:500H_2O. To be specific, the required TEOS and TPAOH were dropped in a flask and stirred at 80 °C for 24 h. Then, sodium hydroxide and aluminum nitrate solution were dropped into the above flask and continued to stir for 5.5 h at 80 °C. The obtained homogeneous gel was transferred to a Teflon-lined stainless-steel autoclave and crystallized at 170 °C for 24 h. The resultant sample was washed with distilled water, filtered, dried overnight at 100 °C, and then calcined at 550 °C in air for 6 h.

H-form zeolites were obtained through ion-exchanging the as-calcined zeolites three times with 0.8 mol L^{-1} NH_4Cl solution at 80 °C for 3 h, which were then dried overnight and calcined at 550 °C for 6 h. The obtained sample was named NZ-60 according to the SiO_2/Al_2O_3 ratio in the synthetic gel. For comparison purposes, ZSM-5 with low acid density (named NZ-240) was synthesized in a similar way by adjusting the SiO_2/Al_2O_3 ratio at 240.

In order to regulate the acid density and acid types, NZ-60 was treated with hot steam at 430 °C and 0.5 MPa. Typically, 1.2 g of NZ-60 with 80−100 mesh was packed into the constant temperature zone of the reaction tube. After increasing the temperature and pressure to 430 °C and 0.5 MPa in a N_2 flow of 35 mL min^{-1}, deionized water was fed into the reactor with a flow of 0.074 mL min^{-1} by a high precision metering pump. The time for hot steam treatment was 10 h. The obtained sample was named SNZ-60.

In order to improve the aromatics selectivity, the Zn promoter was introduced into the above three samples by the incipient wetness impregnation method. Typically, 0.092 g of zinc nitrate was dissolved in 2.0 g of water and then added into 2.0 g of catalyst, followed by ultrasonication for 30 min, leaving for 4 h at room temperature, and drying overnight at 100 °C. Finally, the samples were calcined at 550 °C for 4 h to form active Zn species. The obtained samples were named Zn/NZ-60, Zn/SNZ-60, and Zn/NZ-240.

Catalyst Characterization. X-ray diffraction (XRD) patterns were recorded on a Rigaku D/Max 2500 diffractometer (40 kV, 100 mA) with Cu Kα (λ = 1.541862 nm) to identify the topology structure of zeolite. The spectra were acquired in the 2θ range of 5.0−50.0° at a scanning rate of 20 ° min^{-1}.

Transmission electron microscopy (TEM) was used to observe morphologies and structures of the samples on a JEM-2100F instrument operated at 200 kV.

N_2 physisorption was used to acquire the surface areas and pore volumes of zeolite. The information was obtained on a Beishide 3H-2000PS2 instrument at −196 °C. Before measurement, the samples were degassed at 250 °C for 4 h. The surface area was calculated by the Brunauer−Emmett−Teller (BET) method. The pore size distribution was obtained

https://doi.org/10.1021/acs.iecr.2c03873
Ind. Eng. Chem. Res. 2023, 62, 1865−1876

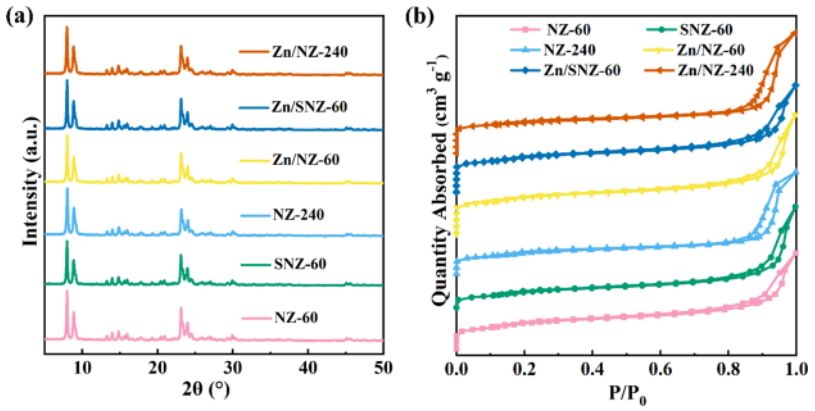

Figure 1. (a) XRD patterns and (b) N_2 adsorption−desorption isotherms of the prepared catalyst.

by the Barrett−Joyner−Halenda (BJH) method, and the pore volume was derived from the t-plot method.

Temperature-programmed desorption of NH_3 (NH_3-TPD) was used to measure the strength and density of acid sites. The information was analyzed on a Micromeritics Autochem II 2920 apparatus. The sample (0.1 g) was first pretreated at 550 °C for 90 min in a He flow and then cooled to 120 °C. Saturated adsorption of NH_3 on the sample was achieved by introducing gaseous NH_3 (15 vol % in helium, 50 mL min^{-1}) into the sample tube for 30 min. To get the NH_3-TPD profile, the sample was then heated from 120 to 550 °C at a ramp of 10 °C min^{-1}. The desorbed NH_3 during heating was monitored by a thermal conductivity detector (TCD).

Pyridine adsorption Fourier transform infrared spectroscopy (Py-IR) was used to characterize the amounts of Brønsted and Lewis acid sites. The information was collected on a Bruker Tenso 27 FT-IR spectrometer. The sample (25 mg) was directly pressed into thin wafers, which was mounted into a vacuum cell. Prior to the measurement, the sample cell was evacuated to 10^{-2} Pa at 400 °C for 60 min then cooled to room temperature. After that, pyridine was adsorbed on the sample for 30 min and then degassed for 30 min under vacuum to remove the excess pyridine. Finally, Py-IR spectra were recorded at room temperature and the concentration of Brønsted and Lewis acid sites was calculated by integrating the absorption peaks at 1540 and 1450 cm^{-1}, respectively.

Diffuse-reflectance infrared transform spectroscopy (DRIFTS) was used to analyze the changes of species in the reaction process. The spectrum was recorded on a Bruker Tensor 27 spectrometer. The catalyst was first activated at 450 °C in 10 mL min^{-1} nitrogen flow for 30 min and then cooled to 350 °C. Methanol was then introduced into the DRIFTS cell and the spectrum of the reaction process was recorded.

^{27}Al nuclear magnetic resonance (^{27}Al NMR) was used to analyze the different structures of aluminum species. The information was acquired on an Agilent 600DD2 spectrometer operating at a Larmor frequency of 600 MHz.

Thermogravimetric (TG) analysis was conducted in the air atmosphere on a NETZSCH STA 449F5 thermogravimetric instrument at a heating rate of 10 °C min^{-1}. The coke content was determined by the weight percentage of coke deposited in the spent catalyst, and the coke formation rate was given as the coke content divided by the lifetime.

Gas chromatography−mass spectrometry (GC−MS) was used to analyze the retained coke species in the spent samples that were carried out at 430 °C for 5 h. The spent sample (20 mg) was dissolved in 1.0 mL of HF solution (10%) to release the organic species trapped in the catalyst, which were then extracted with 1 mL of dichloromethane and analyzed on GC8890-5977B with an HP-5MS capillary column.

Methanol to Aromatics Performance Evaluation. Methanol to aromatics performance test was evaluated in a fixed-bed stainless-steel tubular reactor (Figure S1). In a typical run, 0.6 g of zeolites with 80−100 mesh was loaded and activated at 450 °C and 0.5 MPa for 1 h in a nitrogen flow (35 mL min^{-1}). After that, the reactions were carried out at 430 °C and 0.5 MPa, where methanol was pumped into the reactor with a methanol weight hourly space velocity (WHSV) of 8 h^{-1}, and nitrogen was used as a diluting gas (35 mL min^{-1}). The gas and liquid products were separated with a cold trap. The methanol conversion and gas-phase products could be analyzed on a Zhongkehuifen GC-7820 gas chromatograph, which was equipped with a flame ionization detector (FID) connected with a 50 m HF-PLOT Al_2O_3/S capillary column and a TCD connected with a 3 m Porapak Q packed column. The liquid products could be analyzed on a Shimadzu GC-2014C chromatograph, which was equipped with an HP-PONA chromatographic column.

RESULTS AND DISCUSSION

Physical Properties of the Catalysts. As shown in Figure 1a, the synthesized parent NZ-60 and NZ-240 exhibited the MFI topology structure according to their five typical diffraction peaks at 2θ = 8−10° and 22−25°.[38−40] The reduction of the diffraction peak intensity for SNZ-60 illustrated decreased relative crystallinity after steam treatment compared with that of NZ-60.[41] The diffraction peak intensity is almost unchanged for the Zn-modified sample, reflecting a minor effect on the crystal structure from Zn introduction.[42] N_2 adsorption−desorption results are shown in Figure 1b, and all samples showed a sharp uptake at the low-pressure region (P/P_0 < 0.01), indicating their microporous structures. The existence of intercrystallite mesopores formed by stacked nanocrystals could also be confirmed for all samples by the presence of an H4 hysteresis loop at a relatively high-pressure area (P/P_0 = 0.9).[43,44] Steam treatment could destroy part of the microporous structure. As a result, the specific surface area of SNZ-60 decreased slightly from 385 to 355 m^2 g^{-1}(Figure 1b and Table 1). In addition, the specific surface area further decreased after introducing Zn species, which was attributed to the blocking effect of Zn species in micropores.

https://doi.org/10.1021/acs.iecr.2c03873
Ind. Eng. Chem. Res. 2023, 62, 1865−1876

Table 1. Textural Properties of Different Nano-ZSM-5 Zeolites

sample	surface area (m^2 g^{-1})			pore volume (cm^3 g^{-1})		
	S_{BET} [a]	S_{Micro} [b]	S_{Exter} [c]	V_{Total} [d]	V_{Micro} [e]	V_{Meso} [f]
NZ-60	385	300	85	0.43	0.14	0.29
SNZ-60	355	271	84	0.47	0.13	0.34
NZ-240	323	264	60	0.46	0.13	0.32
Zn/NZ-60	371	289	82	0.47	0.14	0.33
Zn/SNZ-60	349	272	77	0.42	0.13	0.29
Zn/NZ-240	305	229	76	0.48	0.11	0.37

[a] S_{BET} calculated by the BET method. [b] S_{Micro} measured by the t-plot method. [c] S_{Meso} calculated by the formula of $S_{Meso} = S_{Total} - S_{Micro}$. [d] V_{Total} determined by N_2 adsorption volume at $P/P_0 = 0.99$. [e] V_{Micro} mesured by the t-plot method. [f] V_{Meso} calculated by the formula of $V_{Meso} = V_{Total} - V_{Micro}$.

TEM images in Figure 2 showed that the crystals of NZ-60 and NZ-240 present a "coffin-like" morphology with a size of about 100 nm. Compared with NZ-60, the morphology of SNZ-60 was not changed after steam treatment. For Zn dispersion on HZSM-5, three kinds of Zn species usually exist, including large ZnO clusters on the external surface, small ZnO clusters within the micropores, and $ZnOH^+$ ions within the skeleton structure.[45] Generally, $ZnOH^+$ could be formed through the reaction between BAS and Zn^{2+}.[46] Therefore, the high acid density could promote the formation of $ZnOH^+$ and alleviate the agglomeration of Zn species. From the TEM and STEM images (Figures 2 and S2) of three Zn-modified catalysts, no obvious Zn particles were observed, which reflected a high dispersion of Zn species because of the low Zn loading (1.0%) and relatively high acid density of the parent ZSM-5.

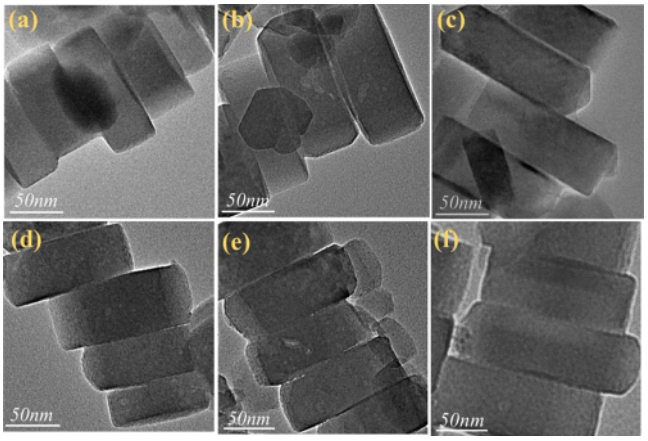

Figure 2. TEM images of the different ZSM-5, (a) NZ-60, (b) SNZ-60, (c) NZ-240, (d) Zn/NZ-60, (e) Zn/SNZ-60, and (f) Zn/NZ-240.

Acid Properties of the Catalysts. The influence of steam treatment on the framework aluminum structure of NZ-60 was revealed by the results of ^{27}Al NMR. As shown in Figure 3a,b, significant peak signals could be observed for NZ-60 and SNZ-60 at about 55−60 and 0 ppm, corresponding to the tetrahedral framework Al (FAl) and octahedral extra-framework Al (EFAl).[47] The steam treatment increased the percentage of EFAl from 8.92 to 12.66%. The new peak at about 30 ppm was attributed to penta-coordination aluminum (Al^{IV}), which was caused by tetrahedral Al coordination distortion.[48] As shown in Figure 3c,d, tetrahedral Al signals

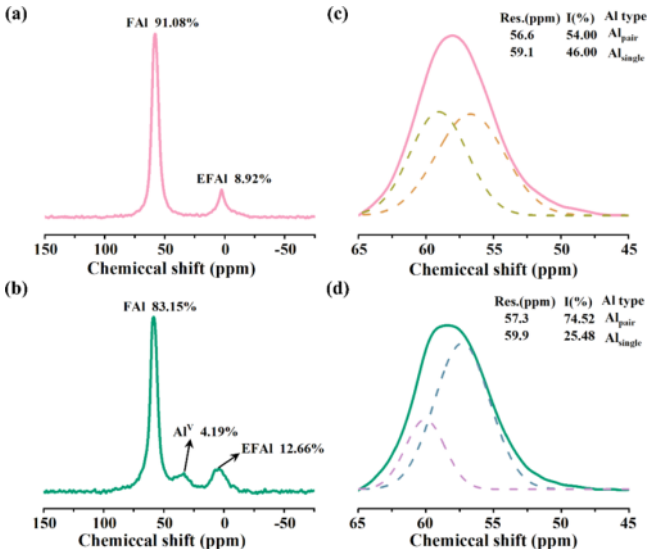

Figure 3. ^{27}Al NMR spectra of (a)NZ-60 and (b) SNZ-60, curve fittings of ^{27}Al MAS NMR spectra of (c)NZ-60 and (d) SNZ-60.

could be fitted with paired Al atom (Al_{pair}) signals at about 57 ppm and isolated Al atom (Al_{single}) signals at about 59 ppm.[49] It could be seen that the percentage of Al_{single} was decreased from 46.00 to 25.48% along with an increase of Al_{pair} percentage from 54.00 to 74.52% after steam treatment. This indicated that Al_{single} could be removed more easily during steam treatment.

Figure 4 and Table 2 show the NH_3-TPD results. Two NH_3 desorption peaks could be observed in the low temperature region of about 200 °C and the high temperature region of about 400 °C for these six samples, which represented the weak and strong acids, respectively.[50,51] After Gaussian function fitting, the specific acid density for weak acid, medium strong acid, and strong acid could be obtained. As shown in Table 2, the density of weak acid and strong acid was 0.13 and 0.29 mmol g^{-1} for NZ-60, respectively, and the total acid density was 0.50 mmol g^{-1}. In contrast, the acid density of SNZ-60 was reduced to 0.25 mmol g^{-1} because of the steam treatment, which could be mainly attributed to the decrease of strong acid density from 0.29 to 0.11 mmol g^{-1}. It was worth noting that the total acid density of NZ-240 with a SiO_2/Al_2O_3 ratio of 125 was also 0.25 mmol g^{-1}, but the strong acid density was higher than that of SNZ-60. Moreover, the introduction of Zn species could obviously change the acid properties of the above-mentioned catalysts. For NZ-60 and NZ-240, the introduction of Zn species significantly reduced the acid density from 0.50 and 0.25 mmol g^{-1} to 0.35 and 0.11 mmol g^{-1}, respectively, which was mainly attributed to the reduction of strong acid sites. Furthermore, the density of weak acid sites increased from 0.13 and 0.04 mmol g^{-1} to 0.17 and 0.05 mmol g^{-1}, respectively. Differently, the change was not found for SNZ-60 on the total acid density and the value remained 0.25 mmol g^{-1}, but the weak acid density increased with the decrease of strong acid density.

Combined with the Py-IR results, the acid type of all catalysts was further clarified. As shown in Figure 5a,b, the peak at 1545 cm^{-1} represented Brønsted acid sites (BAS), and the peak at 1454 cm^{-1} represented Lewis acid sites (LAS).[42] The acid density of BAS and LAS was 31.8 and 22.0 μmol g^{-1} for NZ-60, respectively, and the B/L ratio was 1.40. After the steam treatment, the content of BAS for SNZ-60 was reduced

https://doi.org/10.1021/acs.iecr.2c03873
Ind. Eng. Chem. Res. 2023, 62, 1865−1876

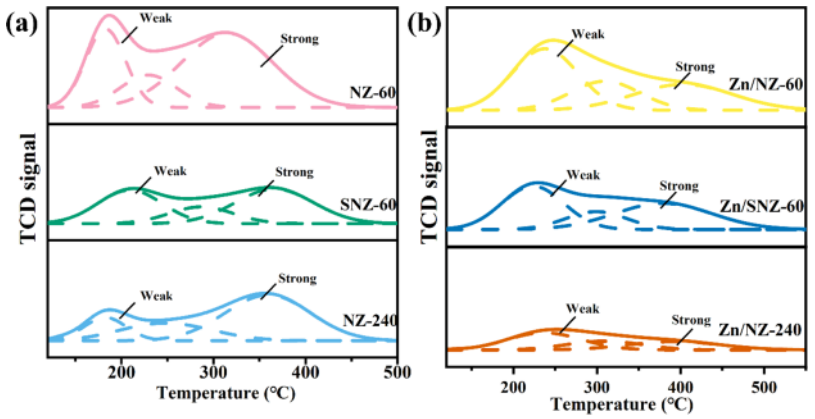

Figure 4. NH_3-TPD profiles for (a) the fresh NZ-60, SNZ-60, NZ-240 and (b) the fresh Zn/NZ-60, Zn/SNZ-60, Zn/NZ-240.

Table 2. Acidic Properties of Different Nano-ZSM-5 Zeolites

sample	SiO_2/Al_2O_3[a]	acidity by strength[b]/mmol g^{-1}				acidity by type[c]/μmol g^{-1}		
		weak	medium	strong	total	Brønsted	Lewis	B/L
NZ-60	61	0.13	0.08	0.29	0.50	31.8	22.0	1.40
SNZ-60		0.09	0.05	0.11	0.25	26.8	24.7	1.08
NZ-240	125	0.04	0.06	0.15	0.25	38.4	7.00	5.50
Zn/NZ-60		0.17	0.08	0.10	0.35	23.2	38.0	0.61
Zn/SNZ-60		0.11	0.04	0.10	0.25	19.5	61.7	0.32
Zn/NZ-240		0.05	0.03	0.03	0.11	14.6	26.0	0.56

[a]Obtained by XRF. [b]Obtained by NH_3-TPD. [c]BAS, LAS, and B/L, obtained by Py-IR. C(pyridine on B sites) = 1.88 IA(B) R^2/W, C(pyridine on L sites) = 1.88 IA(L) R^2/W (R = 6.5 mm, W = 30 mg).

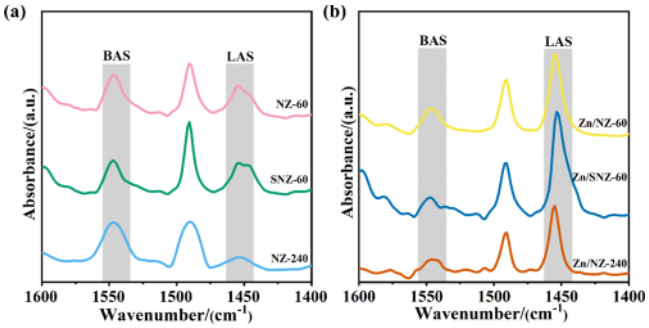

Figure 5. Py-IR spectra for (a) the fresh NZ-60, SNZ-60, NZ-240 and (b) the fresh Zn/NZ-60, Zn/SNZ-60, Zn/NZ-240.

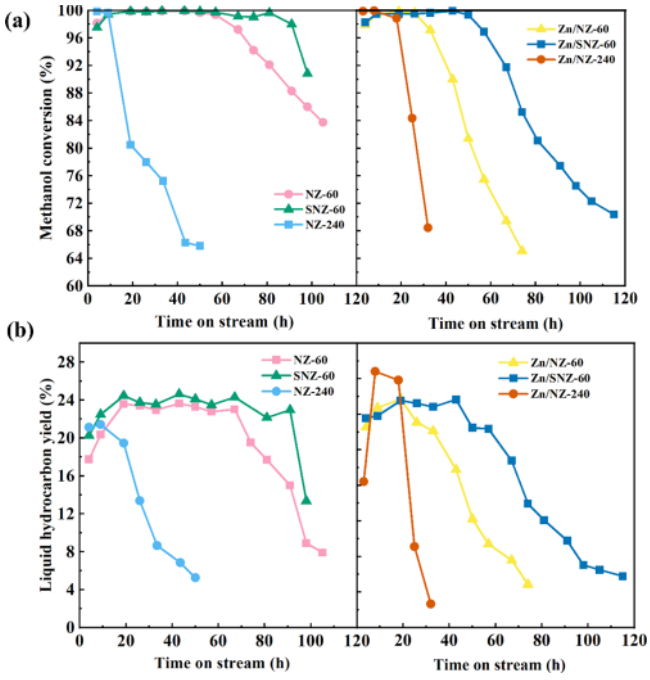

Figure 6. (a) Methanol conversion and (b) liquid hydrocarbon yield with time on steam of the prepared catalyst.

to 26.8 μmol g^{-1} accompanied by an increase of LAS to 24.7 μmol g^{-1}, which also reduced the B/L ratio to 1.08. For the NZ-240 with the same acid density as the SNZ-60, the ratio of B/L reached 5.50, which was attributed to the high density of BAS (38.4 μmol g^{-1}) and the low density of LAS (7.00 μmol g^{-1}). The introduced Zn species could react with surface acid sites to form Zn-LAS. Therefore, the density of LAS was increased to 38.0, 61.7, and 26.0 μmol g^{-1} for Zn/NZ-60, Zn/SNZ-60, and Zn/NZ-240, respectively, and the corresponding density of BAS was decreased to 23.2, 19.5, and 14.6 μmol g^{-1}, which significantly reduced the B/L ratio. It should be noted that the acid density of Zn/SNZ-60 was not changed after Zn introduction. This may be attributed to the different Zn-LAS structure on Zn/SNZ-60, which can be indicated by its more obviously increased LAS compared with that on Zn/NZ-60(Table 2) after Zn introduction.

MTA Performance. As shown in Figure 6a,b, these catalysts had significant differences in catalytic stability. For NZ-60, ~100% methanol conversion and ~24% liquid hydrocarbon yield could be maintained for about 65 h, and then, the slow catalyst deactivation occurred in the next 40 h due to the gradual coke deposition and pore blockage. In contrast, the steam treatment on NZ-60 slowed the deactivation of the catalyst; 100% methanol conversion could

https://doi.org/10.1021/acs.iecr.2c03873
Ind. Eng. Chem. Res. 2023, 62, 1865−1876

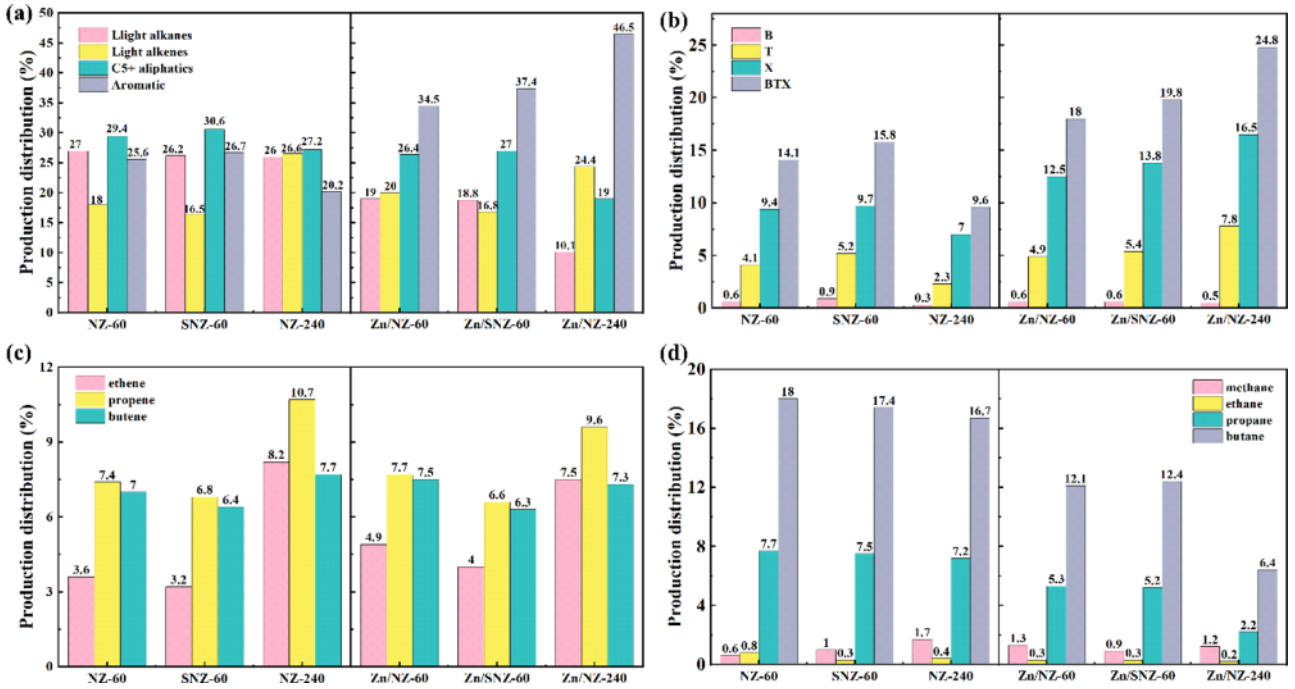

Figure 7. (a) Product selectivity, (b) BTX selectivity, (c) alkenes selectivity, and (d) alkane selectivity of the prepared catalyst.

be maintained for about 90 h over SNZ-60. Moreover, the liquid hydrocarbon yield was slightly increased. In view of the fact that no obvious change on the physical properties of SNZ-60 could be found compared with NZ-60 (XRD and TEM result), the significantly reduced acidity (NH_3-TPD result) after steam treatment indicated that the acid sites with low acid density could complete the conversion of methanol to aromatics with high catalytic stability.

However, the realization of such a catalytic role for acid sites cannot do without the LAS, which could be inferred from the catalytic performance of NZ-240. Although the NZ-240 also had an acid density of 0.25 mmol g^{-1}, poor catalytic performance was found. Methanol conversion and liquid hydrocarbon yield decreased gradually with time on steam, and the total catalytic life was only about 50 h with the maximum yield of liquid hydrocarbon of only 22%. The specific acid properties of NZ-240 are shown in Figure 5 and Table 2, and it could be found that the acid sites are mainly BAS (38.4 μmol g^{-1}) and the B/L ratio reached 5.50, much higher than 1.08 for SNZ-60. Although the presence of BAS with this high density could promote the aromatization process, the deep polymerization of aromatics for the formation of coke precursors could also be aggravated, which caused the rapid deactivation of NZ-240. In contrast, the density of LAS for SNZ-60 could reach 24.7 μmol g^{-1}, which was much higher than that 7 μmol g^{-1} of NZ-240. Li and co-workers[52] found that these LAS could promote the formation of a series of unsaturated oxygenates containing the C−C bond (acetic acid, acetaldehyde, and acetone etc.) with the participation of BAS, which could be rapidly involved in the initiation of the MTA conversion. To be specific, unsaturated aldehydes/ketones could be converted into alkenes via the decarbonylation route or cracking route, thus initiating the alkene cycle. In addition, the cyclic unsaturated ketones could be converted to aromatics via protonation, dehydration, and isomerization, thus initiating the aromatic cycle. Therefore, the aromatization process still occurred normally under this low acid density with more LAS. It is worth noting that BAS could catalyze the aromatization process via the cyclization, deprotonation, and hydride transfer steps. Not only that, the deep aromatization process is also promoted when the acid density of BAS is high. Therefore, it is easy to understand that the deep aromatization process over SNZ-60 could be inhibited because of the lower density of BAS, which determined a higher catalytic stability.

For Zn-modified ZSM-5 catalysts, the introduction of Zn could consume some BAS, and induce the formation of Zn-LAS, which could suppress the hydrogen transfer process and promote the dehydrogenation aromatization process during the catalytic reaction.[3] This could obviously promote the formation of aromatics but inevitably accelerate catalyst deactivation. This was because that the formed Zn-LAS could promote the alkylation of benzene and toluene, resulting in an increase of heavy aromatics for coke formation. For Zn/NZ-60, the acid density of BAS was decreased from 31.8 to 23.2 μmol g^{-1} of parent NZ-60 (Table 2) and the LAS density increased from 22 to 38 μmol g^{-1}. Because of the enhanced aromatization process, methanol conversion could be maintained at ∼100% for only 30 h, and the total catalytic lifetime was 76 h, which was significantly lower than 105 h of NZ-60. Similarly, the introduction of Zn on NZ-240 also increased the acid density of LAS at the sacrifice of BAS and the catalytic life was reduced to about 30 h, shorter than 50 h of NZ-240. In addition, no obvious increase in the maximum liquid hydrocarbon yield (∼24%) could be found for Zn/NZ-60 after the Zn modification. In contrast, the maximum liquid hydrocarbon yield over Zn/NZ-240 can reach 27%, much higher than 22% of parent NZ-240. This remarkable increase was probably associated with a more significant change in BAS and LAS density, as shown in Table 2.

However, good catalytic stability was still presented for Zn/SNZ-60. 100% methanol conversion and 24% liquid hydrocarbon yield could be maintained for 50 h, the total catalyst life reached up to 120 h, much longer than that of Zn/NZ-60. This indicated that the implementation of steam treatment before

https://doi.org/10.1021/acs.iecr.2c03873
Ind. Eng. Chem. Res. 2023, 62, 1865−1876

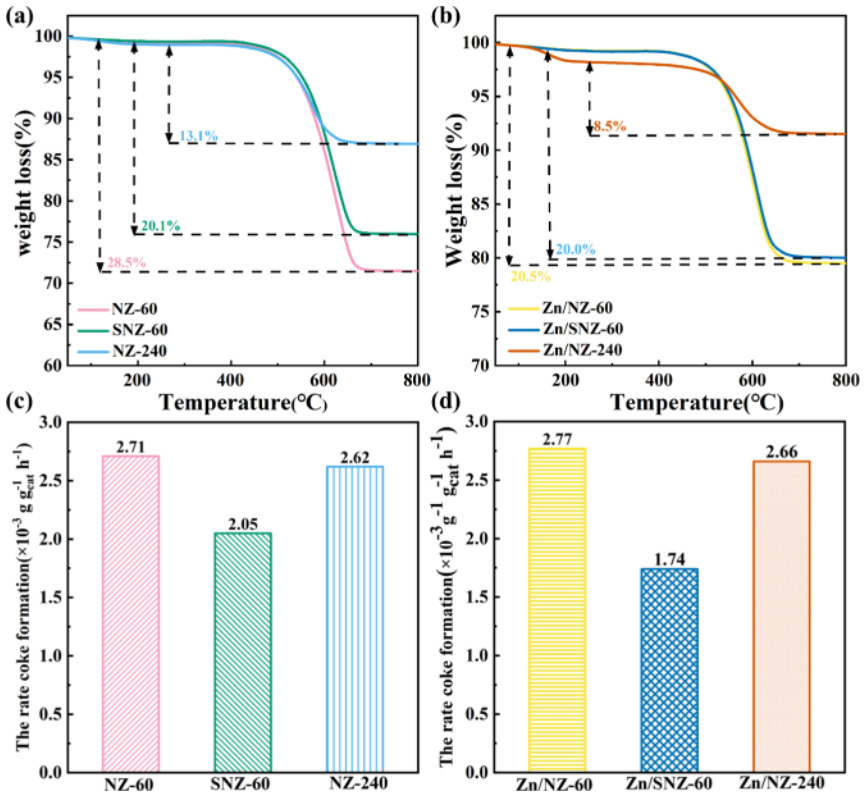

Figure 8. (a, b) TG results and (c, d) the rate of coke formation of deactivated catalysts.

Zn introduction is an important measure to improve the catalytic stability for ZSM-5 catalysts. For the possible reasons behind, it was found that the acid density of Zn/SNZ-60 was not changed compared with parent SNZ-60 and remained at 0.25 mmol g^{-1}. This was obviously different from that for Zn/NZ-60 and Zn/NZ-240, whose acid density was obviously lower than that of parent ZSM-5 (Table 2). Therefore, the maintenance of acid density after Zn introduction is the key to maintain high catalytic stability.

The difference of product selectivity over these catalysts could also reflect the obvious effect of acid properties. As shown in Figure 7, in view of the strong hydrogen transfer on NZ-60 with high acid density, the selectivity of light alkanes and light alkenes was attained to 27 and 18%, respectively. Correspondingly, the total aromatics selectivity and BTX selectivity were 25.6 and 14.1% for NZ-60, respectively. Although the acid density was decreased after steam treatment, the aromatic selectivity of SNZ-60 still reached 26.7%, and the selectivity of BTX was also increased to 15.8%. These results indicated that the aromatization process could be achieved at very low acid density. One important thing to notice is that the increase of the Al_{pair} percentage for SNZ-60 (^{27}Al NMR) could enhance hydrogen transfer reactions, which was also beneficial to the formation of aromatics.

By contrast, the NZ-240 had the same acid density as SNZ-60, but the product was dominated by light alkenes with a selectivity of 26.6%. Moreover, the selectivity of aromatic and BTX was only 20.2 and 9.6%, respectively. Combined with the difference of the acid type between SNZ-60 and NZ-240, the difference of aromatic selectivity further indicated that the high density of LAS on SNZ-60 played a positive role during the aromatic production. The introduction of Zn species could consume part of BAS on the surface, and the new generated Zn-LAS could obviously promote the dehydrogenation aromatization process of alkenes, the selectivity of total aromatics, and BTX could increase from 25.6 and 14.1% to 34.5 and 18% of NZ-60, respectively.[53] In addition, the selectivity of light alkanes was significantly decreased from 27 to 19%. Interestingly, the introduction of Zn species on SNZ-60 with low acid density also significantly improved aromatics selectivity, which was increased from 26.7 to 37.4%, higher than the NZ-60. It is noteworthy that the addition of Zn species reduced the density of BAS from 26.8 to 19.5 μmol g^{-1}, while the LAS was increased from 24.7 to 61.7 μmol g^{-1}, which determined a much lower B/L ratio. Therefore, a small amount of BAS could coordinate with a large amount of LAS to achieve sufficient aromatization, while the catalyst deactivation was inhibited due to the inhibited polyaromatic generation induced by BAS. Surprisingly, the aromatic selectivity of the Zn-modified NZ-240 could reach 46.5%, which was not only higher than Zn/NZ-60 but also higher than Zn/SNZ-60. This result further revealed that a small amount BAS was enough for the aromatic generation, and the sufficient LAS, especially Zn-LAS, was necessary.

The coke deposition over spent ZSM-5 catalysts was studied by TG characterization (Figure 8). For NZ-60 with a total life of 105 h, the coke content could reach 28.5 wt %, and the coke formation rate was 2.71 × 10^{-3} g g_{cat}^{-1} h^{-1}. After steam treatment, the coke deposition content and coke formation rate of spent SNZ-60 were, respectively, decreased to 20.1% and 2.05 × 10^{-3} g g_{cat}^{-1} h^{-1}, reflecting the positive effect of steam treatment on the anti-coke deposition performance. For spent NZ-240 with the catalytic life of only 50 h, the coke content was only 13.1%. However, the coke deposition rate reached 2.62 × 10^{-3} g g_{cat}^{-1} h^{-1}. The acid density of NZ-240 was the same with that of SNZ-60, but NZ-240 had more BAS,

https://doi.org/10.1021/acs.iecr.2c03873
Ind. Eng. Chem. Res. 2023, 62, 1865−1876

which could promote the aromatization process. Correspondingly, deep alkylation of aromatics to heavy aromatics could also be strengthened, which obviously increased the carbon deposition rate. For Zn/NZ-60 and Zn/NZ-240, the coke content of the used catalysts was reduced, while the coke deposition rate was increased. In contrast, no significant change on coke content could be found for used Zn/SNZ-60. However, the coke rate was significantly reduced to 1.74 × 10^{-3} g g_{cat}^{-1} h^{-1}, which determined a longer catalytic lifetime.

GC−MS was carried out (Figure 9) to analyze the organic species retained in spent catalysts. As could be seen from

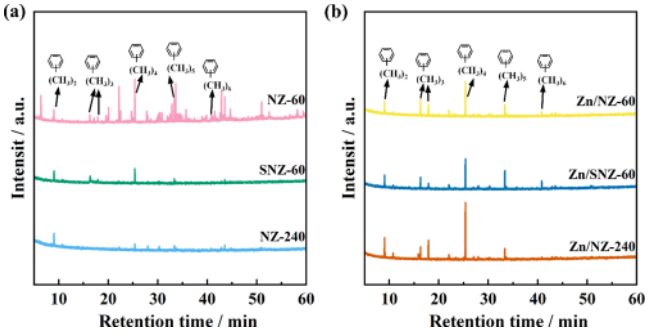

Figure 9. GC−MS chromatograms of the organic extracts from (a) the spent NZ-60, SNZ-60, NZ-240, and (b) the spent Zn/NZ-60, Zn/SNZ-60, Zn/NZ-240 after the MTA reaction at 430 °C for 5 h.

Figure 9, polymethylbenzenes (trimethylbenzenes, tetramethylbenzenes, and pentamethylbenzenes) were the main soluble coke species. Compared with that of NZ-60, the GC−MS signals were much lower for SNZ-60 and NZ-240, suggesting that a weak reaction process occurred on SNZ-60 and NZ-240 due to their lower acid density. After the introduction of Zn species, the intensity of signals of long-chain alkanes was apparently weakened for Zn/NZ-60 because of the inhibition of the hydrogen transfer process. For Zn/SNZ-60 and Zn/NZ-240, the induction of Zn species promoted the formation of hydrocarbon pools species, and the signals of methylbenzene were dramatically increased. These results were conformed to the results of reaction performance. Specifically, after the introduction of Zn species, for all the catalysts (Zn/NZ-60, Zn/SNZ-60, and Zn/NZ-240), the selectivity of aromatic obviously increased, whereas the selectivity of alkanes exhibited the inverse trend.

In situ DRIFTS measurements were carried out to reveal the microscopic reaction process of the MTA reaction over above ZSM-5 catalysts with different acid properties (Figures 10, S3, and S4). For NZ-60 with high total acid density and BAS density, the adsorbed methanol could be rapidly converted to dimethyl ether (DME) species and further decomposed to the surface methoxy species (SMS), which could be confirmed by the dramatically enhanced peaks at 3009 cm^{-1}, 2968 cm^{-1} (stretching vibration of the C−H bond for hydrogen-bonded DME), and 2867 cm^{-1} (stretching vibration of the C−H bond for SMS absorbed on BAS).[54−56] After 4 min, the new bands at 2922 cm^{-1} ascribed to olefinic cations were appeared and gradually enhanced.[57] In addition, peaks at 3125, 1510 cm^{-1} (belonged to the dimethylcyclopentenyl (DMCP) cationic species), and 1615 cm^{-1} (attributed to the aromatic species) also gradually appeared as the time goes on.[56−59] Accompanied by these, the peaks at 3600 cm^{-1} attributed to the bridge hydroxyl group (BAS) was obviously reduced, indicating that the BAS was the main adsorption sites for these species and active centers for methanol conversion.[60] Interestingly, the intensity of the peaks attributed to methanol (2955 and 2852 cm^{-1}) was very weak throughout the experiment, which suggested that the conversion of methanol was very fast over the NZ-60 catalyst with high BAS density.[54,55]

When a part of BAS was removed by water vapor (SNZ-60), the rate of methanol conversion was significantly attenuated. As shown in Figure 10c, the intensity of peaks attributed to the adsorbed methanol (2955 and 2852 cm^{-1}) was obviously stronger than that of DME species (3009 and 2968 cm^{-1}), SMS (2867 cm^{-1}), and olefinic cations (2922 cm^{-1}). Moreover, no bands at 3125, 1510, and 1615 cm^{-1} could be found during the reaction. The above results indicated that the absorbed unsaturated species (aromatics, olefinic) were reduced due to the decrease of Brønsted acid sites for SNZ-60, which corresponded to the weaker GC−MS signals of organic species than that of NZ-60. However, as for NZ-240, which possessed the same amount of acid sites with that SNZ-60 but more BAS, the intensity of olefinic cations (2922 cm^{-1}) was signally stronger than that of adsorbed methanol (2955 and 2852 cm^{-1}). The bands ascribed to the DMCP cationic (3125, 1510 cm^{-1}) and aromatic species (1615 cm^{-1}) could also be found, which indicated that the BAS was the main adsorption centers and active centers for the reactive species in methanol aromatization. However, because of the low acid density of NZ-240, the intensity of these bands was still weaker than that of NZ-60.

After the introduction of Zn, part of BAS was transformed into Zn-Lewis acid, which signally promotes the formation of olefinic, DMCP species, and aromatics by enhancing the dehydrogenation. However, the intensity of adsorption bands for the carbocation of these species was apparently reduced due to the decrease of Brønsted acid sites. As shown in Figures 10b,f, S3b,f, and S4b,f, for Zn/NZ-60 and Zn/NZ-240, the intensities of the peaks at 2922, 3125, 1510, and 1615 cm^{-1} were lower than that of their corresponding parent ZSM-5. Accompanied by this, the bands attributed to DME species (3009 and 2968 cm^{-1}) and SMS (2867 cm^{-1}) were also slightly weakened, while more obvious bands attributed to adsorbed methanol (2955 and 2852 cm^{-1}) could be observed. These results indicated that dehydration and decomposition of methanol were suppressed to some extent due to the reduction of BAS. Interestingly, although the BAS content of Zn/SNZ-60 was less than that of SNZ-60, which had the same acid density as SNZ-60, the peaks at 2922 (attributed to olefinic cations) were obviously higher than that of SNZ-60. The result implied that the Zn-Lewis acid sites with strong dehydrogenation properties could promote the formation of olefins. Compared to NZ-240 with the same acid density but higher BAS density, the bands attributed to adsorbed methanol (2955 and 2852 cm^{-1}) were also enhanced, further indicating that the preliminary conversion of methanol was slightly restrained due the lack of BAS.

Combining the evaluation results, it can be concluded that both the BAS and Lewis acid played an important role in methanol conversion. For BAS, it was the main active center and adsorption centers for methanol aromatization. Not only can it catalyze the dehydration and decomposition of methanol to generate DME and SMS species but it can also promote the formation of olefins and aromatics through participating in a series of oligomerization, hydrogen transfer, and dehydrocyclization. However, because of the weak dehydration property

https://doi.org/10.1021/acs.iecr.2c03873
Ind. Eng. Chem. Res. 2023, 62, 1865−1876

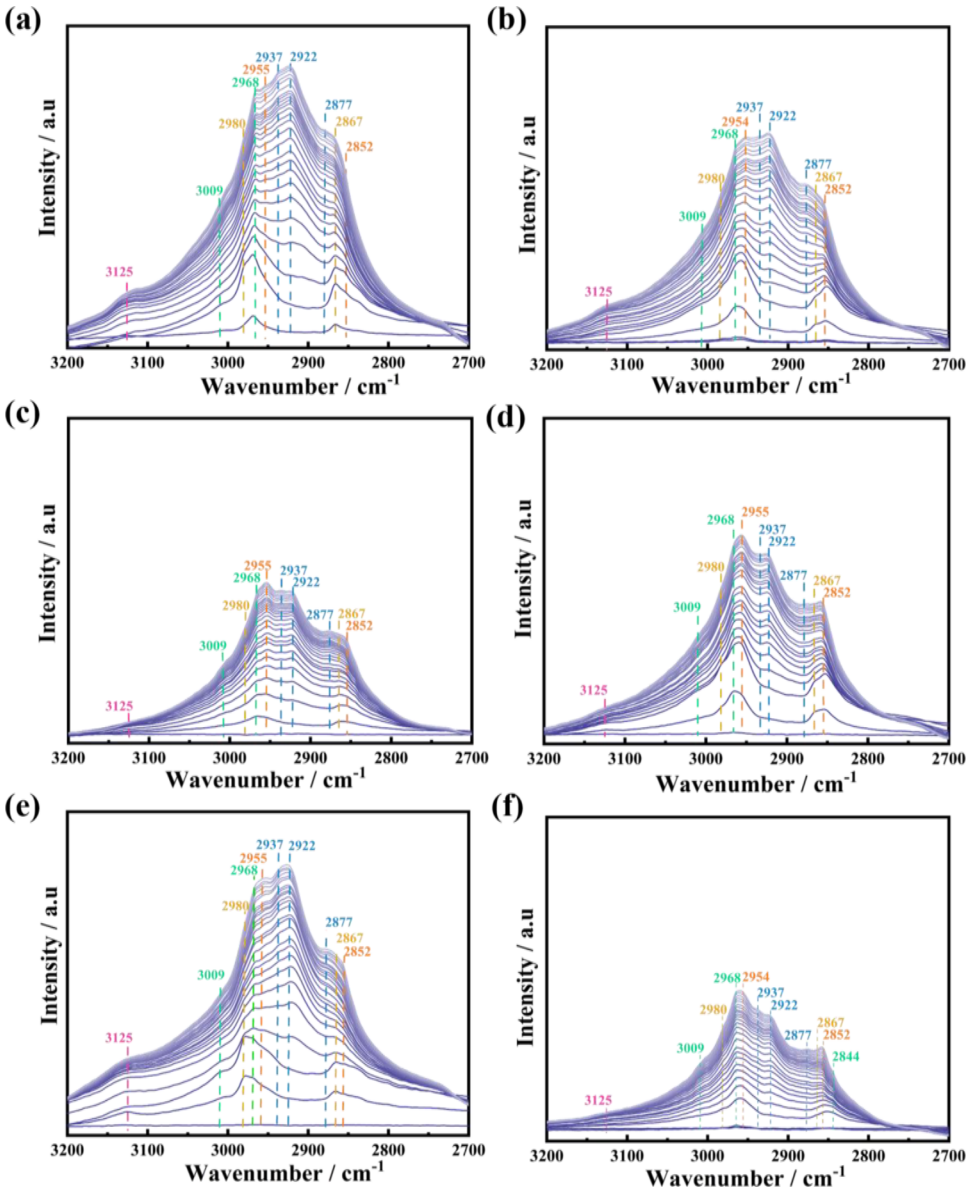

Figure 10. In situ DRIFTS results over different ZSM-5 (a) NZ-60, (b) Zn/NZ-60, (c) SNZ-60, (d) Zn/SNZ-60, (e) NZ-240, and (f) Zn/NZ-240.

and strong adsorption capacity for unsaturated species, simply increasing the BAS could not only improve the olefin selectivity in the final products but also promote the coke deposition and the catalyst deactivation (confirmed by the results of NZ-60 and NZ-240). Different with BAS, Zn-LAS presented a positive role in the formation of aromatics due to its strong dehydrogenation property. Thus, introducing some amount of Zn species could improve the aromatic selectivity, although the BAS was dramatically reduced for Zn-modified ZSM-5. In addition, although the Al-LAS (nonframework aluminum) was difficult to catalyze the dehydrocyclization process, it could replace part of BAS to catalyze the generation of aromatic intermediates through the aldol cycle and indirectly promote the generation of aromatics. More importantly, the weak adsorption of Al-LAS to aromatic species apparently inhibited the formation of coke species such as polymethylbenzene, which could improve catalytic stability.

The above real-time DRIFT tracking of surface species over ZSM-5 with different acid properties allowed us to reveal the evolving process of the active organics. As shown in Figure 11, the acidic proton could first catalyze the conversion of adsorbed methanol into DME and the SMS, then the formed SMS reacted with DME or methanol to form initial olefins, olefinic species, together with the following formed DMCP and aromatic species.

CONCLUSIONS

In summary, highly stable methanol aromatization was achieved on Zn/ZSM-5 prepared by preliminary steam treatment before Zn introduction. It was found that steam treatment destroyed part of the framework of ZSM-5 with a SiO_2/Al_2O_3 ratio of 60. The acid density decreased significantly from 0.5 to 0.25 mmol g^{-1}, and the B/L decreased from 1.40 to 1.08. However, its aromatization performance could still be maintained with a similar lifetime as parent ZSM-5. This indicated that low density of acid sites could complete methanol aromatization with high catalytic stability. Nevertheless, comparative experiment showed that the realization of

https://doi.org/10.1021/acs.iecr.2c03873
Ind. Eng. Chem. Res. 2023, 62, 1865−1876

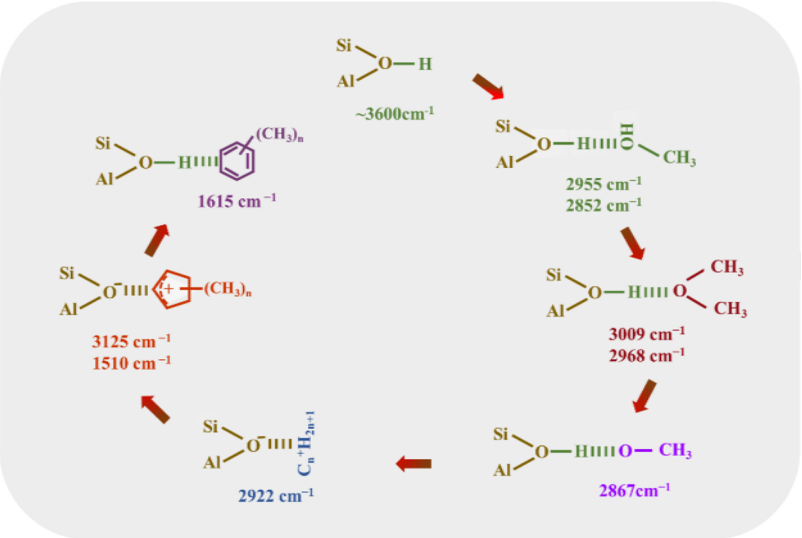

Figure 11. Dynamic evolving trajectories of surface-active species.

such a catalytic role for acid sites could not be achieved without LAS participation. Adjusting the SiO_2/Al_2O_3 ratio from 60 to 240 could also decrease acid density to 0.25 mmol g^{-1}, but BAS-dominated acid sites (B/L = 5.5) promoted the coke formation and reduced the lifetime to 50 h. This reflected that Al-LAS and BAS on steam-treated ZSM-5 provided synergistic catalysis for stable aromatization, and a small amount of BAS could coordinate with certain amount of LAS to achieve stable aromatization. The acid density of steam-treated ZSM-5 could be well maintained after introducing Zn species, which determined an increased aromatics selectivity and a quite different well-maintained stability. The result that Zn/NZ-240 presented a much higher aromatics selectivity than Zn/NZ-60 and Zn/SNZ-60 further revealed that a small amount BAS was enough for aromatization, and the sufficient LAS, especially Zn-LAS, was necessary. GC−MS results further confirmed that the reduction of acid density after steam treatment could significantly inhibit the formation of coke precursors, which improved the catalytic stability. The introduction of Zn species could inhibit hydrogen transfer and promote the dehydrogenation process, which accelerated the formation of coke precursors and shortened the catalytic lifetime. In situ DRIFTS measurements also reflected synergistic catalysis of BAS, Al-LAS, and Zn-LAS for stable MTA.

■ ASSOCIATED CONTENT

Supporting Information

The Supporting Information is available free of charge at https://pubs.acs.org/doi/10.1021/acs.iecr.2c03873.

Schematic drawing of the reaction process system for MTA; STEM mapping results for the Zn-modified catalyst; and in situ DRIFTS spectra over different ZSM-5 (PDF)

■ AUTHOR INFORMATION

Corresponding Authors

Tingjun Fu − *State Key Laboratory of Clean and Efficient Coal Utilization, College of Chemical Engineering and Technology, Taiyuan University of Technology, Taiyuan 030024 Shanxi, China*; orcid.org/0000-0001-9799-7457; Email: futingjun@tyut.edu.cn

Li Zhang − *Key Laboratory of Magnetic Molecules and Magnetic Information Materials (Ministry of Education), School of Chemistry and Material Science, Shanxi Normal University, Taiyuan 030031 Shanxi, China*; Email: zhangli603606@163.com

Zhong Li − *State Key Laboratory of Clean and Efficient Coal Utilization, College of Chemical Engineering and Technology, Taiyuan University of Technology, Taiyuan 030024 Shanxi, China*; orcid.org/0000-0001-6087-6854; Email: lizhong@tyut.edu.cn

Authors

Chuntao Cao − *State Key Laboratory of Clean and Efficient Coal Utilization, College of Chemical Engineering and Technology, Taiyuan University of Technology, Taiyuan 030024 Shanxi, China*

Liangliang Zhang − *State Key Laboratory of Clean and Efficient Coal Utilization, College of Chemical Engineering and Technology, Taiyuan University of Technology, Taiyuan 030024 Shanxi, China*

Qian Ma − *State Key Laboratory of Clean and Efficient Coal Utilization, College of Chemical Engineering and Technology, Taiyuan University of Technology, Taiyuan 030024 Shanxi, China*

Zhenjun Xu − *State Key Laboratory of Clean and Efficient Coal Utilization, College of Chemical Engineering and Technology, Taiyuan University of Technology, Taiyuan 030024 Shanxi, China*

Ran Wang − *State Key Laboratory of Clean and Efficient Coal Utilization, College of Chemical Engineering and Technology, Taiyuan University of Technology, Taiyuan 030024 Shanxi, China*

Han Li − *State Key Laboratory of Clean and Efficient Coal Utilization, College of Chemical Engineering and Technology, Taiyuan University of Technology, Taiyuan 030024 Shanxi, China*

Complete contact information is available at: https://pubs.acs.org/10.1021/acs.iecr.2c03873

https://doi.org/10.1021/acs.iecr.2c03873
Ind. Eng. Chem. Res. 2023, 62, 1865−1876

Notes

The authors declare no competing financial interest.

■ ACKNOWLEDGMENTS

This study was financially supported by the National Natural Science Foundation of China (No. 21878207, No. 21978191) and the Scientific and Technological Innovation Programs of Higher Education Institutions in Shanxi Province (2019).

■ REFERENCES

(1) Dai, C.; Du, K.; Chen, Z.; Chen, H.; Guo, X.; Ma, X. Synergistic Catalysis of Multi-Stage Pore-Rich H-BZSM-5 and Zn-ZSM-5 for the Production of Aromatic Hydrocarbons from Methanol via Lower Olefins. *Ind. Eng. Chem. Res.* **2020**, *59*, 20693−20700.

(2) Pan, D.; Song, X.; Yang, X.; Gao, L.; Wei, R.; Zhang, J.; Xiao, G. Efficient and selective conversion of methanol to para-xylene over stable H[Zn,Al]ZSM-5/SiO2 composite catalyst. *Appl. Catal. A-Gen.* **2018**, *557*, 15−24.

(3) Zhang, G. Q.; Bai, T.; Chen, T. F.; Fan, W. T.; Zhang, X. Conversion of Methanol to Light Aromatics on Zn-Modified Nano-HZSM-5 Zeolite Catalysts. *Ind. Eng. Chem. Res.* **2014**, *53*, 14932−14940.

(4) Li, T.; Shoinkhorova, T.; Gascon, J.; Ruiz-Martínez, J. Aromatics Production via Methanol-Mediated Transformation Routes. *ACS Catal.* **2021**, *11*, 7780−7819.

(5) Lim, Y. H.; Gim, M. Y.; Kim, H.; Kim, D. H. Top-down HCl treatment to prepare highly active Ga species in Ga/ZSM-5 for propane aromatization. *Fuel Process. Technol.* **2022**, *227*, No. 107107.

(6) Wei, Z.; Chen, L.; Cao, Q.; Wen, Z.; Zhou, Z.; Xu, Y.; Zhu, X. Steamed Zn/ZSM-5 catalysts for improved methanol aromatization with high stability. *Fuel Process. Technol.* **2017**, *162*, 66−77.

(7) Zhang, Y.; Qu, Y.; Wang, D.; Zeng, X. C.; Wang, J. Cadmium Modified HZSM-5: A Highly Efficient Catalyst for Selective Transformation of Methanol to Aromatics. *Ind. Eng. Chem. Res.* **2017**, *56*, 12508−12519.

(8) Olah, G. A. Beyond oil and gas: the methanol economy. *Angew. Chem. Int. Ed.* **2005**, *44*, 2636−2639.

(9) Bi, Y.; Wang, Y.; Chen, X.; Yu, Z.; Xu, L. Methanol aromatization over HZSM-5 catalysts modified with different zinc salts. *Chinese. J. Catal.* **2014**, *35*, 1740−1751.

(10) Valecillos, J.; Vicente, H.; Gayubo, A. G.; Aguayo, A. T.; Castaño, P. Spectro-kinetics of the methanol to hydrocarbons reaction combining online product analysis with UV−vis and FTIR spectroscopies throughout the space time evolution. *J. Catal.* **2022**, *408*, 115−127.

(11) Jin, R.; Hu, H.; Wang, J.; Zhang, Z.; Dai, C.; Ma, X. SAPO-34 and Zn/ZSM-5 synergistic catalysis of methanol to aromatics from light olefins. *New J. Chem.* **2022**, *46*, 8443−8450.

(12) Liu, M.; Cui, T.; Guo, X.; Li, J.; Song, C. Stable Zn@ZSM-5 catalyst via a dry gel conversion process for methanol-to-aromatics reaction. *Microporous Mesoporous Mater.* **2021**, *312*, No. 110696.

(13) Song, Y.; Zhang, L.; Li, G.; Shang, Y.; Zhao, X.; Ma, T.; Zhang, L.; Zhai, Y.; Gong, Y.; Xu, J.; Deng, F. ZSM-5 extrudates modified with phosphorus as a super effective MTP catalyst: Impact of the acidity on binder. *Fuel Process. Technol.* **2017**, *168*, 105−115.

(14) Wang, Y.; An, H.; Ma, H.; Zhang, X.; Kang, G.; Cao, J. Catalytic properties and deactivation behavior of modified H-ZSM-5 in the conversion of methanol-to-aromatics. *Adv. Powder Technol.* **2021**, *32*, 1869−1880.

(15) Su, X.; Zhang, K.; Snatenkova, Y.; Matieva, Z.; Bai, X.; Kolesnichenko, N.; Wu, W. High-efficiency nano [Zn,Al]ZSM-5 bifunctional catalysts for dimethyl ether conversion to isoparaffin-rich gasoline. *Fuel Process. Technol.* **2020**, *198*, No. 106242.

(16) Wang, S.; Wang, P.; Qin, Z.; Chen, Y.; Dong, M.; Li, J.; Zhang, K.; Liu, P.; Wang, J.; Fan, W. Relation of Catalytic Performance to the Aluminum Siting of Acidic Zeolites in the Conversion of Methanol to Olefins, Viewed via a Comparison between ZSM-5 and ZSM-11. *ACS Catal.* **2018**, *8*, 5485−5505.

(17) Che, Q.; Yang, M.; Wang, X.; Chen, X.; Chen, W.; Yang, Q.; Yang, H.; Chen, H. Aromatics production with metal oxides and ZSM-5 as catalysts in catalytic pyrolysis of wood sawdust. *Fuel Process. Technol.* **2019**, *188*, 146−152.

(18) Li, S.; Yang, H.; Wang, S.; Dong, M.; Wang, J.; Fan, W. Facile synthesis of hierarchical macro/microporous ZSM-5 zeolite with high catalytic stability in methanol to olefins. *Microporous Mesoporous Mater.* **2022**, *329*, No. 111538.

(19) Yamaguchi, A.; Jin, D.; Ikeda, T.; Sato, K.; Hiyoshi, N.; Hanaoka, T.; Mizukami, F.; Shirai, M. Deactivation of ZSM-5 zeolite during catalytic steam cracking of n-hexane. *Fuel Process. Technol.* **2014**, *126*, 343−349.

(20) Zhao, L.; Gao, J.; Xu, C.; Shen, B. Alkali-treatment of ZSM-5 zeolites with different SiO_2/Al_2O_3 ratios and light olefin production by heavy oil cracking. *Fuel Process. Technol.* **2011**, *92*, 414−420.

(21) Yang, C.; Qiu, M.; Hu, S.; Chen, X.; Zeng, G.; Liu, Z.; Sun, Y. Stable and efficient aromatic yield from methanol over alkali treated hierarchical Zn-containing HZSM-5 zeolites. *Microporous Mesoporous Mater.* **2016**, *231*, 110−116.

(22) Yang, Y.; Jiang, W.; Jiang, J.; Qiu, Q.; Mao, P.; Wu, M.; Zhang, L. Synthesis of hierarchical ZSM-5 zeolites templated by sodium alginate toward enhanced catalytic activity for esterification. *J Sold. State. Chem.* **2020**, *292*, No. 121686.

(23) Feng, R.; Yan, X.; Hu, X.; Wu, J.; Yan, Z. Direct synthesis of b-axis oriented H-form ZSM-5 zeolites with an enhanced performance in the methanol to propylene reaction. *Microporous Mesoporous Mater.* **2020**, *302*, No. 110246.

(24) Zhang, Y.; Li, M.; Xing, E.; Luo, Y.; Shu, X. Protective desilication of highly siliceous H-ZSM-5 by sole tetraethylammonium hydroxide for the methanol to propylene (MTP) reaction. *RSC Adv.* **2018**, *8*, 37842−37854.

(25) Niu, X.; Gao, J.; Wang, K.; Miao, Q.; Dong, M.; Wang, G.; Fan, W.; Qin, Z.; Wang, J. Influence of crystal size on the catalytic performance of H-ZSM-5 and Zn/H-ZSM-5 in the conversion of methanol to aromatics. *Fuel Process. Technol.* **2017**, *157*, 99−107.

(26) Liu, R.; Zhu, H.; Wu, Z.; Qin, Z.; Fan, W.; Wang, J. Aromatization of propane over Ga-modified ZSM-5 catalysts. *J. Fuel Chem. Technol.* **2015**, *43*, 961−969.

(27) Wang, N.; Qian, W.; Shen, K.; Su, C.; Wei, F. Bayberry-like ZnO/MFI zeolite as high performance methanol-to-aromatics catalyst. *Chem. Commun.* **2016**, *52*, 2011−2014.

(28) Wang, Y.; Dai, C.; Chen, B.; Wang, Y.; Shi, C.; Guo, X. Nanoscale HZSM-5 supported PtAg bimetallic catalysts for simultaneous removal of formaldehyde and benzene. *Catal. Today* **2015**, *258*, 616−626.

(29) Zhang, J.; Qian, W.; Kong, C.; Wei, F. Increasing para-Xylene Selectivity in Making Aromatics from Methanol with a Surface-Modified Zn/P/ZSM-5 Catalyst. *ACS Catal.* **2015**, *5*, 2982−2988.

(30) Zhang, Q.; Tan, J.; Wang, T.; Zhang, Q.; Ma, L.; Qiu, S.; Weng, Y. Sorbitol transformation into aromatics: A comparative evaluation of Ni/HZSM-5 and Ni/Hβ. *Fuel* **2016**, *165*, 152−158.

(31) Zhu, X.; Zhang, J.; Cheng, M.; Wang, G.; Yu, M.; Li, C. Methanol Aromatization over Mg−P-Modified [Zn,Al]ZSM-5 Zeolites for Efficient Coproduction of *para*-Xylene and Light Olefins. *Ind. Eng. Chem. Res.* **2019**, *58*, 19446−19455.

(32) Jin, T.; Zhang, D.; Peng, J.; Wu, Y.; Ma, J.; Zhang, J.; Tian, X.; Ding, M. Pretreatment of HZSM-5 with organic alkali and cobalt: Application in catalytic pyrolysis of lignin to produce monocyclic aromatic hydrocarbons. *Fuel Process. Technol.* **2022**, *233*, No. 107308.

(33) Pinilla-Herrero, I.; Borfecchia, E.; Holzinger, J.; Mentzel, U. V.; Joensen, F.; Lomachenko, K. A.; Bordiga, S.; Lamberti, C.; Berlier, G.; Olsbye, U.; Svelle, S.; Skibsted, J.; Beato, P. High Zn/Al ratios enhance dehydrogenation vs hydrogen transfer reactions of Zn-ZSM-5 catalytic systems in methanol conversion to aromatics. *J. Catal.* **2018**, *362*, 146−163.

(34) Khezri, H.; Izadbakhsh, A.; Izadpanah, A. A. Promotion of the performance of La, Ce and Ca impregnated HZSM-5 nanoparticles in the MTO reaction. *Fuel Process. Technol.* **2020**, *199*, No. 106253.

https://doi.org/10.1021/acs.iecr.2c03873
Ind. Eng. Chem. Res. 2023, 62, 1865−1876

(35) Gao, Y.; Zheng, B.; Wu, G.; Ma, F.; Liu, C. Effect of the Si/Al ratio on the performance of hierarchical ZSM-5 zeolites for methanol aromatization. *RSC Adv.* **2016**, *6*, 83581−83588.
(36) Li, H.; Fu, T.; Zhang, L.; Ma, Q.; Cui, L.; Li, Z. Variance in the catalytic performance of nano-ZSM-5 zeolites during the reaction process of methanol to aromatics and its relation to the structural properties. *J. Fuel Chem. Technol.* **2021**, *49*, 483−494.
(37) Fu, T.; Shao, J.; Li, Z. Catalytic synergy between the low Si/Al ratio Zn/ZSM-5 and high Si/Al ratio HZSM-5 for high-performance methanol conversion to aromatics. *Appl. Catal. B-Environ.* **2021**, *291*, No. 120098.
(38) Zhang, G.; Fan, Y.; Huang, J.; Wang, L.; Yang, C.; Lyu, M.; Liu, H.; Ma, Y. Decoupling nucleation from crystal-growth for the synthesis of nanocrystalline zeolites. *Dalton. Trans.* **2020**, *49*, 7258−7266.
(39) Zhao, X.; Wei, L.; Cheng, S.; Huang, Y.; Yu, Y.; Julson, J. Catalytic cracking of camelina oil for hydrocarbon biofuel over ZSM-5-Zn catalyst. *Fuel Process. Technol.* **2015**, *139*, 117−126.
(40) Tian, J.; Qi, L.; Zhang, Q.; Zhan, G.; Sun, D.; Li, Q. Structure engineering of alveoli-like ZSM-5 with encapsulated Pt nanoparticles for the enhanced benzene oxidation. *Nanoscale* **2022**, *14*, 250−262.
(41) Zhang, S.; Gong, Y.; Zhang, L.; Liu, Y.; Dou, T.; Xu, J.; Deng, F. Hydrothermal treatment on ZSM-5 extrudates catalyst for methanol to propylene reaction: Finely tuning the acidic property. *Fuel Process. Technol.* **2015**, *129*, 130−138.
(42) Zhang, C.; Kwak, G.; Lee, Y.; Jun, K.; Gao, R.; Park, H.; Kim, S.; Min, J.; Kang, S. C.; Guan, G. Light hydrocarbons to BTEX aromatics over Zn-modified hierarchical ZSM-5 combined with enhanced catalytic activity and stability. *Microporous Mesoporous Mater.* **2019**, *284*, 316−326.
(43) Jia, Y.; Shi, Q.; Wang, J.; Ding, C.; Zhang, K. Synthesis, characterization, and catalytic application of hierarchical nano-ZSM-5 zeolite. *RSC Adv.* **2020**, *10*, 29618−29626.
(44) Yang, L.; Liu, Z.; Liu, Z.; Peng, W.; Liu, Y.; Liu, C. Correlation between H-ZSM-5 crystal size and catalytic performance in the methanol-to-aromatics reaction. *Chinese. J. Catal.* **2017**, *38*, 683−690.
(45) Kolyagin, Y. G.; Ordomsky, V. V.; Khimyak, Y. Z.; Rebrov, A. I.; Fajula, F.; Ivanova, I. I. Initial stages of propane activation over Zn/MFI catalyst studied by in situ NMR and IR spectroscopic techniques. *J. Catal.* **2006**, *238*, 122−133.
(46) Zhang, Y.; Wu, S.; Xu, X.; Jiang, H. Ethane aromatization and evolution of carbon deposits over nanosized and microsized Zn/ZSM-5 catalysts. *Catal. Sci. Technol.* **2020**, *10*, 835−843.
(47) Jin, W.; Qiao, J.; Yu, J.; Wang, Y.; Cao, J. Influence of Hollow ZSM-5 Zeolites Prepared by Treatment with Different Alkalis on the Catalytic Conversion of Methanol to Aromatics. *Energy Fuel.* **2020**, *34*, 14633−14646.
(48) Tempelman, C. H. L.; Hensen, E. J. M. On the deactivation of Mo/HZSM-5 in the methane dehydroaromatization reaction. *Appl. Catal. B-Environ.* **2015**, *176-177*, 731−739.
(49) Ong, L. H.; Dömök, M.; Olindo, R.; van Veen, A. C.; Lercher, J. A. Dealumination of HZSM-5 via steam-treatment. *Microporous Mesoporous Mater.* **2012**, *164*, 9−20.
(50) Cui, N.; Guo, H.; Zhou, J.; Li, L.; Guo, L.; Hua, Z. Regulation of framework Al distribution of high-silica hierarchically structured ZSM-5 zeolites by boron-modification and its effect on materials catalytic performance in methanol-to-propylene reaction. *Microporous Mesoporous Mater.* **2020**, *306*, No. 110411.
(51) Zhang, L.; Jiang, Z.; Yu, Y.; Sun, C.; Wang, Y.; Wang, H. Synthesis of core−shell ZSM-5@meso-SAPO-34 composite and its application in methanol to aromatics. *RSC Adv.* **2015**, *5*, 55825−55831.
(52) Yang, L.; Wang, C.; Dai, W.; Wu, G.; Guan, N.; Li, L. Progressive steps and catalytic cycles in methanol-to-hydrocarbons reaction over acidic zeolites. *Fundam. Res.* **2022**, *2*, 184−192.
(53) Wang, N.; Li, J.; Sun, W.; Hou, Y.; Zhang, L.; Hu, X.; Yang, Y.; Chen, X.; Chen, C.; Chen, B.; Qian, W. Rational Design of Zinc/Zeolite Catalyst: Selective Formation of p-Xylene from Methanol to Aromatics Reaction. *Angew. Chem. Int. Ed.* **2022**, *61*, No. e202114786.
(54) Campbell, S. M.; Jiang, X.; Howe, R. F. Methanol to hydrocarbons: spectroscopic studies and the significance of extra-framework aluminium. *Microporous Mesoporous Mater.* **1999**, *29*, 91−108.
(55) Forester, T. R.; Howe, R. F. In situ FTIR studies of methanol and dimethyl ether in ZSM-5. *J. Am. Chem. Soc.* **1987**, *109*, 5076−5082.
(56) Wu, X.; Xu, S.; Wei, Y.; Zhang, W.; Huang, J.; Xu, S.; He, Y.; Lin, S.; Sun, T.; Liu, Z. Evolution of C-C Bond Formation in the Methanol-to-Olefins Process: From Direct Coupling to Autocatalysis. *ACS Catal.* **2018**, *8*, 7356−7361.
(57) Minova, I. B.; Matam, S. K.; Greenaway, A.; Catlow, C. R. A.; Frogley, M. D.; Cinque, G.; Wright, P. A.; Howe, R. F. Elementary Steps in the Formation of Hydrocarbons from Surface Methoxy Groups in HZSM-5 Seen by Synchrotron Infrared Microspectroscopy. *ACS Catal.* **2019**, *9*, 6564−6570.
(58) Mosley, J. D.; Young, J. W.; Agarwal, J.; Schaefer, H. F.; Schleyer, P.; Duncan, M. A. Structural isomerization of the gas-phase 2-norbornyl cation revealed with infrared spectroscopy and computational chemistry. *Angew. Chem. Int. Ed.* **2014**, *53*, 5888−5891.
(59) Shao, S.; Zhang, H.; Xiao, R.; Li, X.; Cai, Y. Catalytic conversion of biomass-derivates by in situ DRIFTS: Evolution of coke. *J. Anal. Appl. Pyrol.* **2017**, *127*, 258−268.
(60) Lin, S.; Zhi, Y.; Chen, W.; Li, H.; Zhang, W.; Lou, C.; Wu, X.; Zeng, S.; Xu, S.; Xiao, J. A.; Zheng, Y.; Wei, Z.; Liu, Z. Liu, Molecular Routes of Dynamic Autocatalysis for Methanol-to-Hydrocarbons Reaction. *J. Am. Chem. Soc.* **2021**, *143*, 12038−12052.

https://doi.org/10.1021/acs.iecr.2c03873
Ind. Eng. Chem. Res. 2023, 62, 1865−1876